

Original Research

Adsorption of Acid Red 88 Anionic Dye from Aqueous Solution onto ZnO/ZnMn₂O₄ Nanocomposite: Equilibrium, Kinetics, and Thermodynamics

Wojciech Konicki^{1*}, Daniel Sibera², Urszula Narkiewicz²

¹Department of Environmental Protection, Maritime University of Szczecin, H. Pobożnego St. 11, 70-507 Szczecin, Poland

²Institute of Chemical and Environment Engineering, West Pomeranian University of Technology, Szczecin, 70-322, Pułaskiego St. 10, Poland

Received: 9 August 2016

Accepted: 29 March 2017

Abstract

The adsorption of acid red 88 (AR88) anionic dye onto ZnO/ZnMn₂O₄ nanocomposite (ZnMn-NC) prepared by the hydrothermal method was carried out. The adsorbent was characterized by means of XRD, SEM, HRTEM, Raman spectroscopy, FTIR, BET, and zeta potential measurements. We investigated the influence of dye initial concentration, temperature, and pH on AR88 adsorption onto ZnMn-NC. Equilibrium data were analyzed by model equations such as Langmuir and Freundlich isotherms and were best represented by the Freundlich isotherm model. The experimental kinetic data were analyzed using pseudo first-order, pseudo second-order, and intraparticle diffusion kinetic models. The adsorption kinetics was best fitted to the pseudo second-order kinetic model. Thermodynamic parameters, change in free energy ΔG° , enthalpy ΔH° , and entropy ΔS° were also evaluated, indicating the spontaneous and exothermic character of the adsorption of AR88 onto ZnMn-NC.

Keywords: adsorption, anionic dye, ZnMn₂O₄, kinetics, thermodynamics

Introduction

Dyes are synthetic organic compounds that are increasingly being produced and used extensively in the paper, leather, textile, plastic, cosmetic, and other industries. Approximately 70,000 ton of dyestuffs are discharged into waste streams each year by the textile industry [1]. The presence of even very low concentrations

of dyes in water reduces light penetration through the water surface, precluding photosynthesis of the aqueous flora. Additionally, many dyes or their metabolites have toxic as well as carcinogenic, mutagenic, and teratogenic effects on aquatic life and humans. Hence, the removal of dyes from aquatic wastewater has become environmentally important.

Various methods including photocatalysis [2], chemical oxidation [3], coagulation [4], electrochemical [5], and adsorption [6] techniques have been applied for the removal of dyes from aqueous solutions. Among these methods, adsorption has been found to be superior

*e-mail: w.konicki@am.szczecin.pl

compared to other techniques for wastewater treatment in terms of its capability to efficiently remove a broad range of pollutants and its simplicity of design. Many adsorbents have been investigated regarding the possibility to lower dye concentrations from such aqueous solutions such as activated carbon [7], carbon nanotubes [8], nanocrystalline magnetic composites [9], graphene [10], fly ash [6], and others [11-13].

One of the most attractive materials is zinc manganese oxide spinel ZnMn_2O_4 , due to its various unique electrochemical [14], photocatalytic [15], optical [16], and magnetic [17] properties. Therefore, various ZnMn_2O_4 nanomaterials with different morphologies such as nanopowders, nanowires, hollow microspheres, and ball-in-ball microspheres have been investigated for application in lithium-ion batteries [18-20], heterogeneous catalysis [21-23], gas sensing [24], and electronic components such as supercapacitors [25] or negative temperature coefficient thermistors [26]. However, to date there have been no studies on the adsorption of dyes onto ZnMn_2O_4 or $\text{ZnO}/\text{ZnMn}_2\text{O}_4$ nanocomposites. Therefore, in the present study we focused our attention on the adsorption of anionic dye acid red 88 onto $\text{ZnO}/\text{ZnMn}_2\text{O}_4$ nanocomposite synthesized by a hydrothermal method. AR88 was selected as an adsorbate for the present study because it is widely used in dyeing textile fabrics, silk, nylon, wool, and leather, and its degradation byproducts have carcinogenic effects. The effects of initial dye concentration, solution pH, and temperature on AR88 adsorption were investigated. The experimental data were analyzed using the pseudo first-order, pseudo-second-order and intraparticle diffusion kinetic models. Langmuir and Freundlich isotherms were employed to quantify the adsorption equilibrium. The thermodynamic parameters of the process, such as enthalpy, entropy and Gibbs free energy, were also determined.

Materials and Methods

Materials

The reactants used for the preparation of ZnMn-NC nanocomposite ($\text{Zn}(\text{NO}_3)_2 \cdot 6\text{H}_2\text{O}$ and $\text{Mn}(\text{NO}_3)_2 \cdot 4\text{H}_2\text{O}$ and KOH) were supplied by Chempur. Anionic dye AR88 ($\text{C}_{20}\text{H}_{13}\text{N}_2\text{NaO}_4\text{S}$, molar mass 400.38) supplied by Zachem Barwniki was used as an adsorbate. The chemical structure of AR88 is shown in Fig. 1. All solutions were prepared using deionized water.

Synthesis of ZnMn-NC

The ZnMn-NC nanocomposite was synthesized by the microwave-assisted hydrothermal method. The nominal concentration of ZnO was 30 wt.% (then 70 wt.% of MnO). At first, a mixture of manganese and zinc hydroxides was obtained by the addition of 2M solution of KOH to 20% solution of a proper amount of $\text{Zn}(\text{NO}_3)_2 \cdot 6\text{H}_2\text{O}$ and $\text{Mn}(\text{NO}_3)_2 \cdot 4\text{H}_2\text{O}$ in water. Such a mixture was then treated

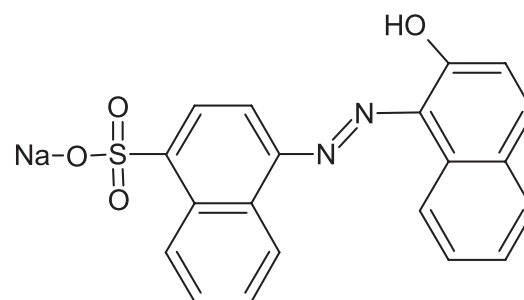


Fig. 1. Molecular structure of AR88.

in the solvothermal microwave reactor. The microwave-assisted synthesis was conducted at 3.8 MPa for 15 min. Next, the obtained material was washed with deionized water to remove salt residues. Finally, the material was dried at 100°C for 24 h.

Characterization Methods

X-ray diffraction (XRD) was conducted on an X'Pert PRO Philips diffractometer using $\text{CuK}\alpha$ radiation. The morphology of the ZnMn-NC was examined by scanning electron microscopy (SEM) Zeiss Supra and high-resolution transmission electron microscopy (HRTEM) on the FEI Tecnai F20 S twin transmission electron microscope. The specific surface area of the ZnMn-NC was determined by the Brunauer-Emmett-Teller (BET) method (nitrogen adsorption) using a Gemini 2360 from Micromeritics. The functional groups on the ZnMn-NC surface were determined using the Fourier transform infrared (FTIR) method (Nicolet iS5 FT-IR Spectrometer, Thermo Scientific). The zeta potential of the sample was determined by a Malvern Instrument Zetasizer 2000 at room temperature. The helium pycnometer AccuPyc 1330 of Micromeritics was applied to determine the density of powder.

Adsorption Experiments

Adsorption experiments were carried out in an Erlenmeyer flask, where the solution (200 mL) with an initial dye concentration was placed. Initial concentrations of AR88 varied from 10 to 50 mg L^{-1} . The flask with AR88 solution was sealed and placed in a temperature-controlled shaking water bath (Grant OLS26 Aqua Pro, Grant Instruments Ltd) and agitated at a constant speed of 160 rpm. To observe the effect of temperature the experiments were carried out at three different temperatures, i.e., 20, 40, and 60°C. Before mixing with the adsorbent, various pH levels of the solution were adjusted by adding a few drops of diluted hydrochloric acid (0.1 N HCl) or sodium hydroxide (0.1 N NaOH). When the desired temperature was reached, about 40 mg of ZnMn-NC was added to the flask. At the end of the equilibrium period 1 ml of aqueous sample was taken from the solution, and the liquid was separated from the adsorbent by centrifugation at 6,000 rpm for

5 min. The determination of AR88 concentration was done spectrophotometrically (GENESYS 10S UV-VIS Spectrometer, Thermo Scientific) at maximum absorbance $\lambda = 505$ nm.

The amount of AR88 adsorbed at equilibrium q_e (mg g^{-1}) was calculated by the following equation:

$$q_e = \frac{(C_0 - C_e)V}{m} \quad (1)$$

...where C_0 (mg L^{-1}) is the initial AR88 concentration, C_e (mg L^{-1}) the AR88 concentration at equilibrium, V (L) the volume of the solution, and m (g) is the mass of the adsorbent.

The procedures of kinetic experiments were identical to those of equilibrium tests. At predetermined moments, aqueous samples were taken from the solution, the liquid was separated from the adsorbent, and the concentration of AR88 in solution was determined spectrophotometrically. The amount of AR88 adsorbed at time t q_t (mg g^{-1}) was calculated by the following equation:

$$q_t = \frac{(C_0 - C_t)V}{m} \quad (2)$$

...where C_t (mg L^{-1}) the AR88 concentration at any time t . Each experiment was carried out in duplicate and the average results are presented. The kinetic and isotherm models were evaluated by the linear correlation coefficient (R^2).

Results and Discussion

Characterization of the Adsorbent

Fig. 2 shows the XRD pattern of ZnMn-NC composites. The sample was composed from two phases: ZnO and ZnMn_2O_4 . The average crystallite size of ZnO and ZnMn_2O_4 calculated by Scherrer equation was 99 and 27 nm, respectively. The morphology of ZnMn-NC

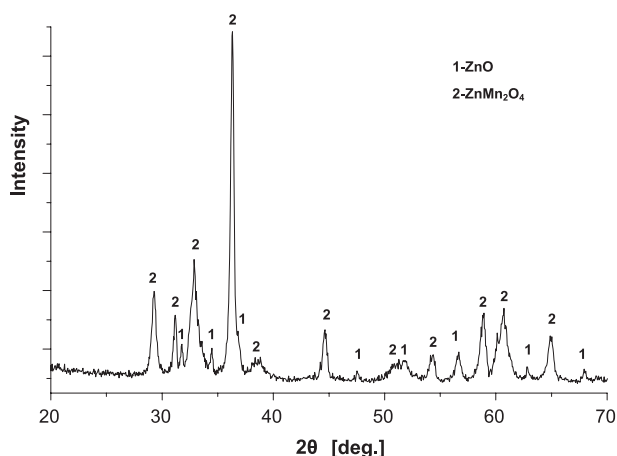


Fig. 2. X-ray diffraction pattern of ZnMn-NC.

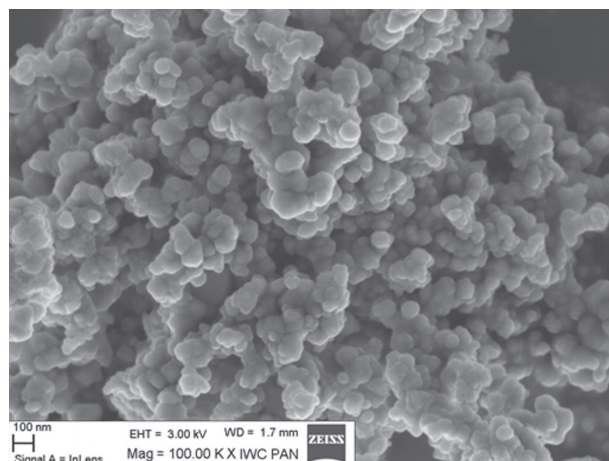


Fig. 3. SEM image of ZnMn-NC.

nanocomposite was investigated using both transmission and scanning electron microscopy. In the SEM image (Fig. 3) only spherical agglomerates can be observed. The agglomeration of the nanoparticles have made image analysis difficult. However, one can suppose that spherical nanocrystals corresponded to the spinel ZnMn_2O_4 phase. TEM images (Figs 4a,b) have shown much more detail.

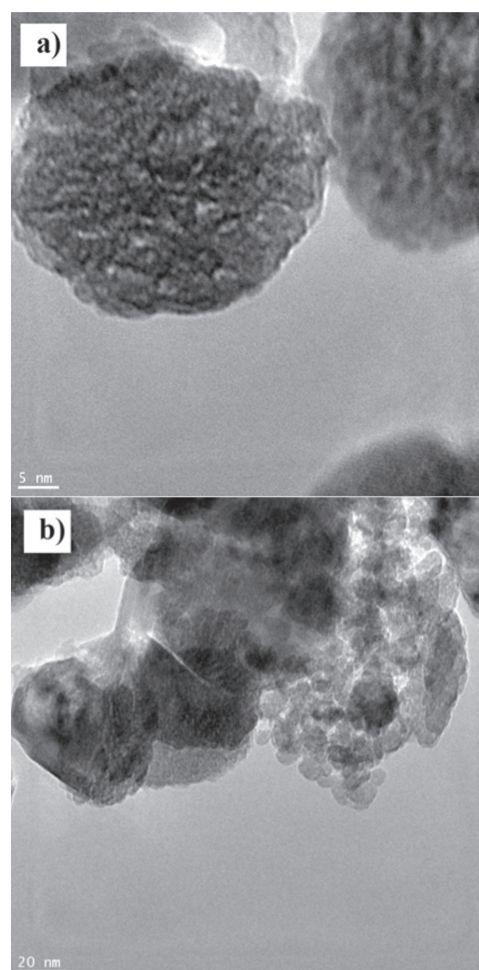


Fig. 4. HRTEM (a, b) images of ZnMn-NC.

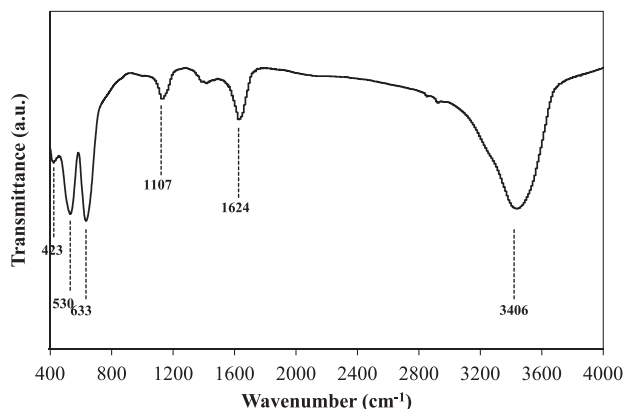


Fig. 5. FTIR spectra of ZnMn-NC.

It can be clearly seen that spherical agglomerates were made up of smaller crystallites. In addition, some much larger crystallites can be observed, probably corresponding to unreacted ZnO. The results of the Raman analysis of the composites were presented elsewhere [27].

Fig. 5 shows the FTIR spectra of ZnMn-NC. The peak at 423 cm^{-1} was assigned to Zn-O stretching vibration [28]. The peaks at 530 and 633 cm^{-1} correspond to the stretching vibration of Mn-O [29]. The peaks in the range of $1,300\text{--}950\text{ cm}^{-1}$ proved the presence of C-O bonds in various chemical surroundings [30]. In addition, the peaks observed at $3,406$ and $1,624\text{ cm}^{-1}$ were ascribed to the stretching vibrations of O-H and the adsorbed water molecules, respectively [31–32].

The BET specific surface area of ZnMn-NC was $25\text{ m}^2\text{g}^{-1}$. The zeta potentials of ZnMn-NC were measured in water solution at pH in the range $3.5\text{--}11.5$, and decreased from positive to negative values with increasing pH over the whole studied range (Fig. 6). The pH_{pzc} of ZnMn-NC was determined as 9.7 . The density of the ZnMn-NC measured using a pycnometer was 4.73 g cm^{-3} .

Effect of Initial Dye Concentration

Fig. 7 shows the effect of the initial dye concentration on adsorption of the AR88 by ZnMn-NC at $\text{pH } 7.0$ and

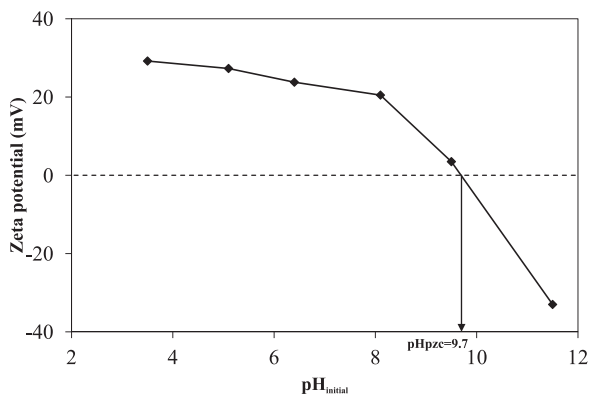


Fig. 6. Effect of pH on zeta potential of ZnMn-NC.

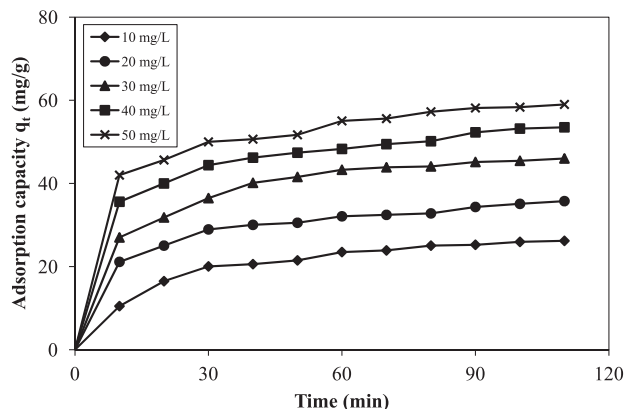


Fig. 7. Effect of initial dye concentration on adsorption capacity of AR88 onto ZnMn-NC. Experimental conditions: $T = 30^\circ\text{C}$, $\text{pH} = 7$.

at 30°C . Initially, the adsorption of AR88 was fast, and then it became slower near the equilibrium. The fast adsorption at the initial stage may be due to the fact that a large number of surface sites are available for adsorption. When the initial dye concentration varied from 10 to 50 mg L^{-1} , the adsorption capacity at equilibrium increased from 26.2 to 59.0 mg g^{-1} . This indicates that the initial dye concentration plays an important role in the adsorption capacity of dye. A higher initial concentration provides an important driving force to overcome all resistances of the dye between the aqueous and solid phases, thus increasing the uptake.

Kinetic Data Analysis

In this study, the adsorption equilibrium data were analyzed using two kinetic models: pseudo first-order and pseudo second-order. The pseudo first-order kinetic model (Eq. 3) and pseudo second-order kinetic model (Eq. 4) are given by the following equations [33]:

$$\ln(q_e - q_t) = \ln q_e - k_1 t \quad (3)$$

$$\frac{t}{q_t} = \frac{1}{k_2 q_e^2} + \frac{1}{q_e} t \quad (4)$$

...where k_1 (min^{-1}) is the pseudo first-order rate constant adsorption, t (min) time, and k_2 ($\text{g mg}^{-1}\text{ min}^{-1}$) is the pseudo second-order rate constant adsorption. Values of k_1 and q_e were calculated from the linear plots of $\ln(q_e - q_t)$ versus t . Values of k_2 and q_e were calculated from the slope and intercept of the linear plots obtained by graphical representation of t/q_t versus t (Fig. 8). Kinetic constants obtained by linear regression for the models and the correlation coefficients R^2 are listed in Table 1. The high values of correlation coefficients R^2 and good agreement between experimental $q_{e,\text{exp}}$ and calculated $q_{e,\text{cal}}$ values indicate that the adsorption system followed the pseudo second-order kinetic model.

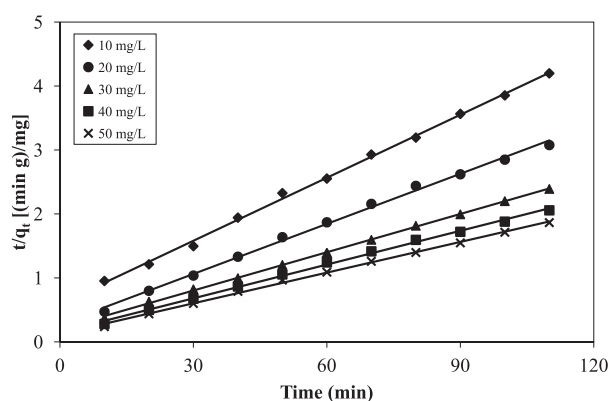


Fig. 8. Pseudo second-order kinetics for adsorption of AR88 onto ZnMn-NC. Experimental conditions: T = 30°C, pH = 7.

Intraparticle Diffusion

To further understand the adsorption of AR88 onto ZnMn-NC, the kinetic behavior of the adsorption process was further analyzed using the intraparticle diffusion model. The intra-particle diffusion model is described as [34]:

$$q_t = k_p t^{0.5} + C \quad (5)$$

...where C (mg g^{-1}) was the intercept and k_p ($\text{mg g}^{-1} \text{min}^{-0.5}$) was the intraparticle diffusion rate constant. According to Eq. (5), if the plot of q_t versus $t^{0.5}$ gave a straight line, then the adsorption process was controlled by intraparticle diffusion and if the data exhibited multi-linear plots, then two or more steps controlled the adsorption process. As shown in Fig. 9, the plots exhibited two linear sections with different slopes, indicating on a two-stage diffusion of AR88 onto ZnMn-NC. The first sharper portion was attributed to the diffusion of dye through the solution to the external surface of adsorbent. The second portion described the gradual adsorption stage, where intraparticle diffusion was rate limiting. Several previous investigations have reported a similar type of plot [13, 35-36].

The values of k_p and C were determined from the slopes of the second linear portion (Table 1). The k_p and C values increased with the initial dye concentration. The

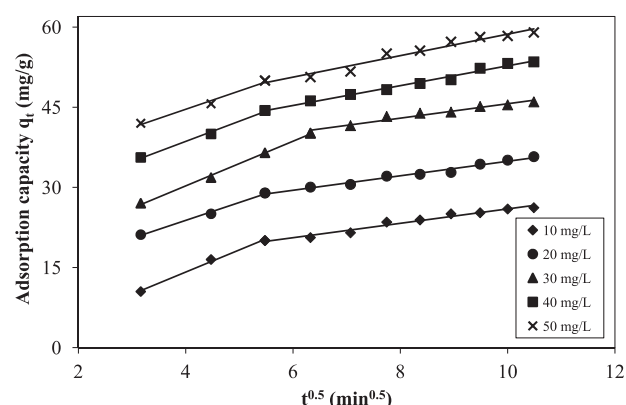


Fig. 9. Intraparticle diffusion model of adsorption of AR88 onto ZnMn-NC. Experimental conditions: T = 30°C, pH = 7.

correlation coefficients of the intraparticle diffusion model are lower than those for the pseudo second-order kinetic model for AR88. This would suggest a predominance of the pseudo second-order adsorption mechanism and a controlling of the overall rate of the dye adsorption process by more than one step.

Adsorption Isotherms

The adsorption data were analyzed using Langmuir's and Freundlich's models. The application of the Langmuir isotherm model is based on monolayer coverage of adsorbent surfaces by the adsorbate. The Freundlich isotherm model is an empirical equation based on the multilayer adsorption of an adsorbate onto heterogeneous surfaces. The well-known linear form of the Langmuir isotherm model is given by the following equation [37]:

$$\frac{C_e}{q_e} = \frac{1}{Q_0 b} + \frac{C_e}{Q_0} \quad (6)$$

...where Q_0 (mg g^{-1}) is the monolayer adsorption capacity and b (L mg^{-1}) is a constant related to energy of adsorption. The values of Q_0 and b were calculated from the slope and intercept of the linear plot C_e/q_e versus C_e . The essential characteristics of the Langmuir isotherm can be expressed

Table 1. Comparison of pseudo first-order, pseudosecond-order, and the intraparticle diffusion models for different initial concentrations of AR88 at 30°C.

C_o (mg L^{-1})	$q_{e,exp}$ (mg g^{-1})	Pseudo first-order model			Pseudo second-order model			Intraparticle diffusion model		
		k_1 (min^{-1})	$q_{e,cal}$ (mg g^{-1})	R^2	k_2 ($\text{g mg}^{-1} \text{min}^{-1}$)	$q_{e,cal}$ (mg g^{-1})	R^2	k_p ($\text{mg g}^{-1} \text{min}^{-0.5}$)	C (mg g^{-1})	R^2
10	26.2	0.0395	25.4	0.938	0.00180	30.5	0.998	1.3469	12.5	0.971
20	35.8	0.0293	20.0	0.927	0.00245	38.3	0.997	1.3562	21.3	0.980
30	46.0	0.0382	29.3	0.987	0.00194	50.3	0.999	1.3520	32.1	0.959
40	53.5	0.0368	32.9	0.850	0.00203	56.8	0.998	1.8548	34.2	0.986
50	59.0	0.0365	31.0	0.954	0.00208	62.5	0.998	2.0100	38.6	0.960

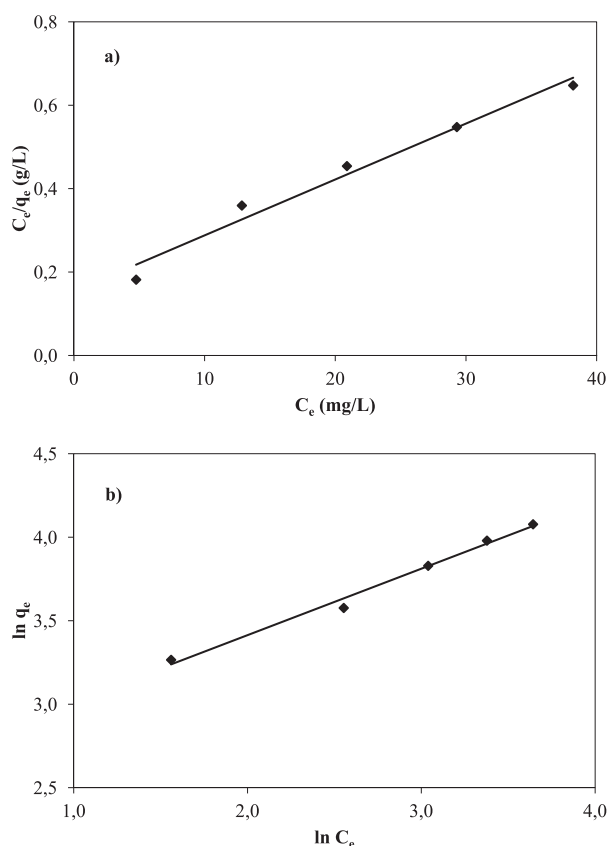


Fig. 10. Langmuir a) and Freundlich b) isotherms for AR8 adsorption onto ZnMn-NC at 30°C.

in terms of dimensionless equilibrium parameter (R_L), which is defined by the following equation:

$$R_L = \frac{1}{1 + bC_0} \quad (7)$$

...where b ($L\ mg^{-1}$) is the Langmuir constant and C_0 ($mg\ L^{-1}$) is the highest initial concentration of the adsorbate. The value of R_L indicates the type of the isotherm to be either unfavorable ($R_L > 1$), linear ($R_L = 1$), favorable ($0 < R_L < 1$), or irreversible ($R_L = 0$).

The Freundlich adsorption isotherm model is expressed by equation as [38]:

$$q_e = K_F C_e^{\frac{1}{n}} \quad (8)$$

A linear form of the Freundlich expression is represented by the following equation:

$$\ln q_e = \ln K_F + \left(\frac{1}{n}\right) \ln C_e \quad (9)$$

...where K_F ($mg\ g^{-1}(L\ mg^{-1})^{1/n}$) and n are Freundlich constants that represent adsorption capacity and adsorption strength, respectively. The values of K_F and n were calculated from the slope and intercept of the linear plot $\ln q_e$ versus $\ln C_e$. The value of n ranging from 1 to 10 indicated that the adsorption process is favourable.

Fig. 10 shows the Langmuir and Freundlich isotherm models for the adsorption of AR88 onto ZnMn-NC. The calculated values of the constants and the correlation coefficients R^2 are given in Table 2. As can be seen, the experimental data better fit the Freundlich model ($R^2 = 0.990$) than the Langmuir model ($R^2 = 0.975$). The R_L value was in the range of 0-1, meanwhile, n for Freundlich isotherm was greater than 1, indicating on favourable adsorption of AR88 onto ZnMn-NC under conditions applied in this study. The value of the maximum adsorption capacity Q_0 of ZnMn-NC in this study was $74.6\ mg\ g^{-1}$. Table 3 lists the comparison of maximum monolayer adsorption capacity of AR88 onto various adsorbents.

Effect of Initial pH

The effect of initial solution pH on adsorption capacity at equilibrium of AR88 onto ZnMn-NC was investigated in the range of pH values from 4.0 to 10.0 at a fixed dyes concentration of $30\ mg\ L^{-1}$ and $30^\circ C$ (Fig. 11). When the initial pH of the dye solution was increased from 4.0 to 10.0, the adsorption capacity decreased from 49.6 to $6.03\ mg\ g^{-1}$. The pHPzc of ZnMn-NC was found to be 9.7, at which point the adsorbent is neutral. Adsorption of cationic dyes was favored at $pH > pHPzc$, while the adsorption of anionic dyes was favored at $pH < pHPzc$. AR88 is anionic azo dye that contains one sulfonic acid group ($R-SO_3Na$). In aqueous solution, the dye dissociates to the sodium ion (Na^+) and the sulfonate anion ($R-SO_3^-$). Therefore, the excess of protons enhances the positive charge of the surface of adsorbent and favours the electrostatic attraction of the dye anions. At acidic pH, the sulfonic groups of dye can be protonated to the neutral form ($R-SO_3H$); however, sulfonic groups exhibit negative charge even at higher acidic solutions due to their pKa values lower than zero [47]. When the pH of the dye solution increases, the number of positively charged sites on surface of the adsorbent decreases and increase the repulsive electrostatic forces between the negatively charged surface of the adsorbent and negatively charged dye molecules, which does not favor

Table 2. Langmuir and Freundlich parameters for the adsorption of AR88 onto ZnMn-NC at 30°C.

Langmuir isotherm			Freundlich isotherm			
Q_0 ($mg\ g^{-1}$)	b ($L\ mg^{-1}$)	R_L	R^2	K_F [($mg\ g^{-1}$)($L\ mg^{-1}$) $^{1/n}$]	n	R^2
74.6	0.087	0.19	0.975	13.7	2.51	0.990

Table 3. Comparison of the maximum monolayer adsorption of AR88 onto various adsorbents.

Adsorbent	Q ₀ (mg g ⁻¹)	Ref.
Bituminous coal	26.1	[39]
Lignite coal	30.09	[39]
Charfines	33.3	[39]
MMWCNTs	54.4	[40]
<i>Azolla microphylla</i>	54.89	[41]
ZnMn-NC	74.6	This study
<i>Azolla rongpong</i>	78.74	[42]
<i>Azolla filiculoides</i>	123.5	[43]
Anion exchange membrane	227.1	[44]
Calcined alunite	832.81	[45]
Natural clay	1,133.10	[46]

the adsorption of AR88 onto ZnMn-NC. Therefore, adsorption of AR88 on the ZnMn-NC surface was more favorable at lower pH.

Effect of Temperature

The effect of temperature on the adsorption capacity of AR88 onto ZnMn-NC was investigated at 20, 40, and 60°C (Fig. 12). It was observed that the adsorption equilibrium of AR88 decreased with the increase in temperature, indicating the exothermic behavior of adsorption.

Thermodynamic parameters such as a change in free energy (ΔG°), enthalpy (ΔH°), and entropy (ΔS°) were determined using the following equations [48]:

$$\ln K_a = \frac{\Delta S^\circ}{R} - \frac{\Delta H^\circ}{R \cdot T} \quad (10)$$

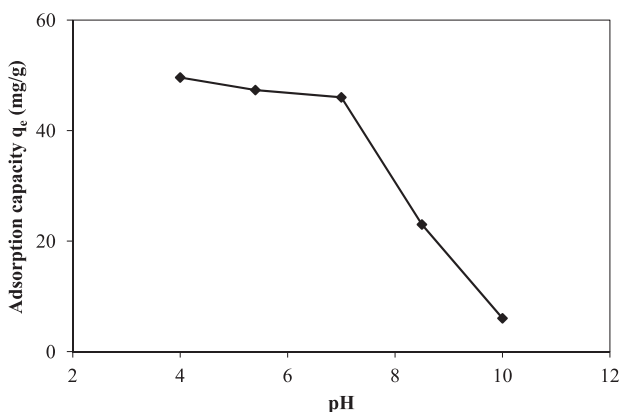


Fig. 11. The effect of initial pH of dye solution on adsorption capacity of AR88 onto ZnMn-NC. Experimental conditions: C_{AR88}^o = 30 mg L⁻¹, T = 30°C.

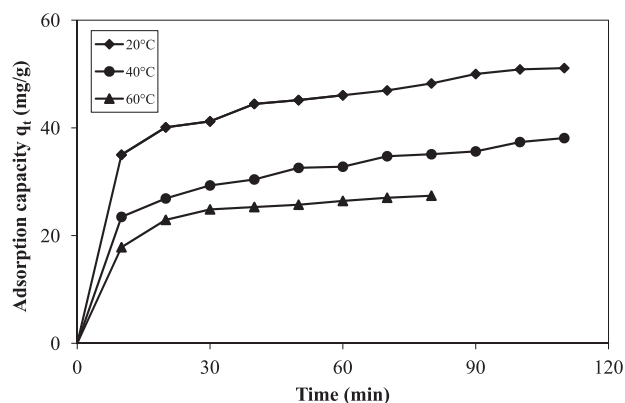


Fig. 12. Effect of temperature on adsorption of AR88 onto ZnMn-NC. Experimental conditions: C_{AR88}^o = 30 mg L⁻¹, pH = 7.

$$K_a = \frac{q_e}{C_e} \quad (11)$$

$$\Delta G^\circ = -RT \ln K_a \quad (12)$$

...where T (K) is the solution temperature and K_a is the adsorption equilibrium constant. Enthalpy (ΔH°) and entropy (ΔS°) were calculated from the slope and intercept from the plot of $\ln q_e/C_e$ versus 1/T (Fig. 13). The value of Gibbs free energy (ΔG°) was calculated using Eq. 12. Thermodynamic parameters are given in Table 4. The negative value of ΔH° indicated the exothermic nature of the adsorption process. The negative value of ΔS° showed the decreased randomness at the solid/solution interface during the adsorption of dye on the active sites of the ZnMn-NC. The ΔG° values were negative at all of the test temperatures, confirming that the adsorption of AR88 onto ZnMn-NC was spontaneous and thermodynamically favorable. The extent of enthalpy ΔH° gave an idea about the type of adsorption, which is mainly physical or chemical. Typically, the adsorption enthalpy of physisorption is lower than 40 kJ mol⁻¹, while that of chemisorption may reach values between 40 and

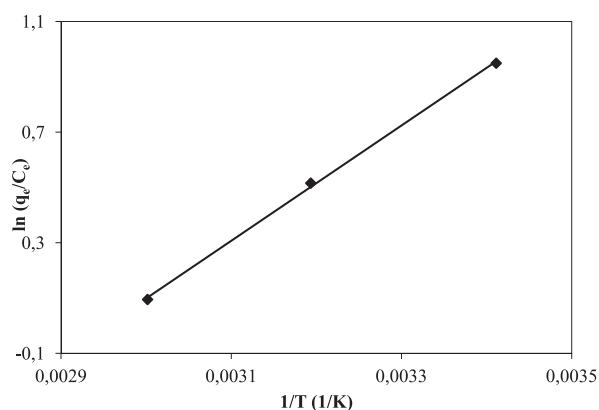


Fig. 13. Van't Hoff plot for the adsorption of AR88 onto ZnMn-NC.

Table 4. Thermodynamic parameters for the adsorption of AR88 onto ZnMn-NC.

Dye concentration (mg L ⁻¹)	ΔH° (kJ mol ⁻¹)	ΔS° (J mol ⁻¹ K ⁻¹)	ΔG° at temperature (°C) (kJ mol ⁻¹)			R ²
			20	40	60	
30	-17.3	-51.2	20	40	60	0.999
			-2.31	-1.34	-0.26	

120 kJ mol⁻¹ [49]. In this study, ΔH° value was in the range of physisorption, indicating the physical nature of the adsorption. The interaction between AR88 and active sites on the ZnMn-NC surface were mainly electrostatic. Generally, the change in free energy for physisorption is between -20 and 0 kJ mol⁻¹ and for chemisorption is in the range of -80 to -400 kJ mol⁻¹ [50]. The values of ΔG° are within the range of -20 to 0 kJ mol⁻¹, indicating physisorption as the predominant mechanism of the adsorption process. These results were in agreement with the finding reported by Amin [7], García et al. [51], Amrhar et al. [52], and Huang et al. [53].

Conclusions

In this study we investigated the adsorption of anionic dye AR88 from aqueous solution onto ZnO/ZnMn₂O₄ (ZnMn-NC) nanocomposites. The kinetic study was performed based on pseudo first-order, pseudo second-order, and intraparticle diffusion kinetic models. The data indicated on the pseudo second-order kinetic model of adsorption kinetics. The adsorption data were analyzed using Langmuir and Freundlich isotherm models. The adsorption data fit the Freundlich isotherm model well. The maximum adsorption capacity calculated from the Langmuir isotherm was 74.6 mg g⁻¹. The thermodynamic parameters showed that the adsorption process of AR88 onto ZnMn-NC was exothermic in nature and spontaneous. The values of ΔH° and ΔG° suggested that the adsorption of AR88 onto ZnMn-NC was a physisorption process.

References

- ATIMTAY A.T., SIKDAR S.K. Security of Industrial Water Supply and Management, Springer Science+Business Media B.V., 2011.
- JAIN R., SHRIVASTAVA M. Photocatalytic removal of hazardous dye cyanosine from industrial waste using titanium dioxide. *J. Hazard. Mater.* **152**, 216, 2008.
- SALEM I.A., EL-MAAZAWI M. Kinetics and mechanism of color removal of methylene blue with hydrogen peroxide catalysed by some supported alumina surfaces. *Chemosphere* **41**, 1173, 2000.
- KASPERCHIK V.P., YASKEVICH A.L., BIL'DYUKEVICH A.V. Wastewater treatment for removal of dyes by coagulation and membrane processes. *Petroleum Chemistry* **52**, 545, 2012.
- KORBAHTI B.K., ARTUT K., GEÇGEL C., ÖZER A. Electrochemical decolorization of textile dyes and removal of metal ions from textile dye and metal ion binary mixtures. *Chem. Eng. J.* **173**, 677, 2011.
- SUN D., ZHANG X., WU Y., LIU X. Adsorption of anionic dyes from aqueous solution on fly ash. *J. Hazard. Mater.* **181**, 335, 2010.
- AMIN N.K. Removal of direct blue-106 dye from aqueous solution using new activated carbons developed from pomegranate peel: Adsorption equilibrium and kinetics. *J. Hazard. Mater.* **165**, 52, 2009.
- KONICKI W., PEŁECH I., MIJOWSKA E., JASINSKA I. Adsorption of anionic dye Direct Red 23 onto magnetic multi-walled carbon nanotubes-Fe₃C nanocomposite: Kinetics, equilibrium and thermodynamics. *Chem. Eng. J.* **210**, 87, 2012.
- WANG L., LI J., WANG Y., ZHAO L., JIANG Q. Adsorption capability for Congo red on nanocrystalline MFe₂O₄ (M = Mn, Fe, Co, Ni) spinel ferrites. *Chem. Eng. J.* **181-182**, 72, 2012.
- RAMESHAG.K., VIJAYAKUMARAA., MURALIDHARA H.B., SAMPATH S. Graphene and graphene oxide as effective adsorbents toward anionic and cationic dyes. *J. Colloid Interface Sci.* **361**, 270, 2011.
- TAHIR S.S., RAUF N. Removal of a cationic dye from aqueous solutions by adsorption onto bentonite clay. *Chemosphere* **63**, 1842, 2006.
- DOGAN M., ABAK H., ALKAN M. Adsorption of methylene blue onto hazelnut shell: Kinetics, mechanism and activation parameters. *J. Hazard. Mater.* **164**, 172, 2009.
- MOUSSAVI G., KHOSRAVI R. The removal of cationic dyes from aqueous solutions by adsorption onto pistachio hull waste. *Chem. Eng. Res. Des.* **89**, 2182, 2011.
- KIM S.W., LEE H.W., MURALIDHARAN P., SEO D.H., YOON W.S., KIM D.K., KANG K. Electrochemical performance and ex situ analysis of ZnMn₂O₄ nanowires as anode materials for lithium rechargeable batteries. *Nano Res.* **4**, 505, 2011.
- ZHAO L., LI X., ZHAO J. Fabrication, characterization and photocatalytic activity of cubic-like ZnMn₂O₄. *Appl. Surf. Sci.* **268**, 274, 2013.
- JAVED Q.U., WANG F., TOUFIQ A.M., RAFIQ M.Y., IQBAL M.Z., KAMRAN M.A. Preparation, characterizations and optical property of single crystalline ZnMn₂O₄ nanoflowers via template-free hydrothermal synthesis. *J. Nanosci. Nanotechnol.* **13** (4), 2937, 2013.
- MENAKA M.Q., LOFLAND S.E., RAMANUJACHARY K.V., GANGULI A.K. Magnetic and photocatalytic properties of nanocrystalline ZnMn₂O₄. *Bull. Mater. Sci.* **32**, 231, 2009.
- COURTEL F.M., ABU-LEBDEH Y., DAVIDSON I.J. ZnMn₂O₄ nanoparticles synthesized by a hydrothermal method as an anode material for Li-ion batteries. *Electrochim. Acta* **71**, 123, 2012.
- CHOI S.H., KANG Y.C. Characteristics of ZnMn₂O₄ Nanopowders Prepared by Flame Spray Pyrolysis for Use as Anode Material in Lithium Ion Batteries. *Int. J. Electrochem. Sci.* **8**, 6281, 2013.

20. BAI Z., FAN N., SUN C., JU Z., GUO C., YANG J., QIAN Y. Facile synthesis of loaf-like $ZnMn_2O_4$ nanorods and their excellent performance in Li-ion batteries. *Nanoscale* **21**, 2442, **2013**.
21. FERRARIS G., FIERRO G., JACONO M.L., INVERSI M., DRAGONE R. A study of the catalytic activity of cobalt-zinc manganites for the reduction of NO by hydrocarbons. *Appl. Catal. B* **36**, 251, **2002**.
22. HENG Y.Z., BIN G., XU Z.C., TENG L. Preparation of $ZnMn_2O_4$ nano-catalyst and its application in synthesizing n-butyl acetate. *Chin. J. Appl. Chem.* **26**, 1315, **2009**.
23. BO W.H., YI C.F., LIANG T.Z., JING L., JUN C. Room-temperature Synthesis and Oxygen-reduction Catalytic Performance of Hollow $ZnMn_2O_4$ Nanospheres and Nanocubes. *Chem. J. Chinese U.* **32**, 595, **2011**.
24. SORITA R., KAWANO T. A highly selective CO sensor: Screening of electrode materials. *Sensor. Actuat. B-Chem.* **36**, 274, **1996**.
25. GAO Y., ZHENG M., PANG H. Achieving High-Performance Supercapacitors by Constructing Porous Zinc-Manganese Oxide Microstructures. *Energy Technol.* **3**, 820, **2015**.
26. GUILLEMET-FRITSCH S., CHANEL C., SARRIAS J., BAYONNE S., ROUSSET A., ALCOBE X., MARTINEZ SARRION M.L. Structure, thermal stability and electrical properties of zinc manganites. *Solid State Ionics* **128**, 233, **2000**.
27. HADZIC B., ROMCEVIC N., ROMCEVIC M., KURYLSZYN-KUDELSKA I., DOBROWOLSKI W., NARKIEWICZ U., SIBERA D. Raman study of surface optical phonons in hydrothermally obtained $ZnO(Mn)$ nanoparticles. *Opt. Mater.* **58**, 317, **2016**.
28. SHAH A.H., MANIKANDAN E., BASHEER AHMED M., GANESAN V. Enhanced Bioactivity of Ag/ZnO Nanorods-A Comparative Antibacterial Study. *J. Nanomed. Nanotechnol.* **4**, 1, **2013**.
29. BASTAMI T.R., ENTEZARI M.H. A novel approach for the synthesis of superparamagnetic Mn_3O_4 nanocrystals by ultrasonic bath. *Ultrason. Sonochem.* **19**, 560, **2012**.
30. STOBINSKI L., LESIAK B., KOVER L., TOTH J., BINIAK S., TRYKOWSKI G., JUDEK J. Multiwall carbon nanotubes purification and oxidation by nitric acid studied by the FTIR and electron spectroscopy methods. *J. Alloys Compd.* **501**, 77, **2010**.
31. TAN X., ZHAO Y., LI G., HU C. Effect of calcination temperature on the structure and hydroxylation activity of $Ni_{0.5}Cu_{0.5}Fe_2O_4$ nanoparticles. *Appl. Surf. Sci.* **257**, 6256, **2011**.
32. CHEN J., HUA ZHU Z., MAA Q., LI L., RUDOLPH V., QING LU G. Effects of pre-treatment in air microwave plasma on the structure of CNTs and the activity of Ru/CNTs catalysts for ammonia decomposition. *Catal. Today* **148**, 97, **2009**.
33. LI L., LIU S., ZHU T. Application of activated carbon derived from scrap tires for adsorption of Rhodamine B. *J. Environ. Sci.* **22**(8), 1273, **2010**.
34. WEBER W.J., MORRIS J.C. Kinetics of adsorption on carbon from solution. *J. Sanit. Eng. Div.* **89**, 31, **1963**.
35. DOGAN M., KARAOGLU M.H., ALKAN M. Adsorption kinetics of maxilon yellow 4GL and maxilon red GRL dyes on kaolinite. *J. Hazard. Mater.* **165**, 1142, **2009**.
36. MA T., CHANG P.R., ZHENG P., ZHAO F., MA X. Fabrication of ultra-light graphene-based gels and their adsorption of methylene blue. *Chem. Eng. J.* **240**, 595, **2014**.
37. LANGMUIR I. The adsorption of gases on plane surfaces of glass, mica and platinum. *J. Am. Chem. Soc.* **40**, 1361, **1918**.
38. FREUNDLICH H. Concerning adsorption in solutions. *Zeitschrift für physikalische Chemie* **57**, 385, **1906**.
39. MOHAN S.V., SAILAJA P., SRIMURALI M., KARTHIKEYAN J. Color Removal of Monoazo Acid Dye from Aqueous Solution by Adsorption and Chemical Coagulation. *Environ. Eng. Policy* **1** (3), 149, **1999**.
40. KONICKI W., PEŁECH I., MIJOWSKA E., JASIŃSKA I. Adsorption Kinetics of Acid Dye Acid Red 88 onto Magnetic Multi-Walled Carbon Nanotubes- Fe_3C Nanocomposite. *Clean* **42** (3), 284, **2014**.
41. PADMESH T.V.N., VIJAYARAGHAVAN K., SEKARAN G., VELAN M. Application of Two- and Three-Parameter Isotherm Models: Biosorption of Acid Red 88 onto Azolla microphylla. *Biorem. J.* **10**, 37, **2006**.
42. PADMESH T.V.N., VIJAYARAGHAVAN K., SEKARAN G., VELAN M. Application of Azolla rongpong on Biosorption of Acid Red 88, Acid Green 3, Acid Orange 7 and Acid Blue 15 from Synthetic Solutions. *Chem. Eng. J.* **122** (1), 55, **2006**.
43. PADMESH T.V.N., VIJAYARAGHAVAN K., SEKARAN G., VELAN M. Batch and Column Studies on Biosorption of Acid Dyes on Fresh Water Macro Alga Azolla filiculoides. *J. Hazard. Mater.* **125** (1-3), 121, **2005**.
44. XING T., KAI H., CHEN G. Study of Adsorption and Desorption Performance of Acid Dyes on Anion Exchange Membrane. *Color. Technol.* **128**, 295, **2012**.
45. AKAR S.T., ALP T., YILMAZER D. Enhanced Adsorption of Acid Red 88 by an Excellent Adsorbent Prepared from Alunite. *J. Chem. Technol. Biotechnol.* **88**, 293, **2012**.
46. AKAR S.T., UYSAL R. Untreated Clay with High Adsorption Capacity for Effective Removal of C.I. Acid Red 88 from Aqueous Solutions: Batch and Dynamic Flow Mode Studies. *Chem. Eng. J.* **162** (2), 591, **2010**.
47. LIMA E.C., ROYER B., VAGHETTI J.C.P., SIMON N.M., DA CUNHA B.M., PAVAN F.A., BENVENUTTI E.V., VESES R.C., AIROLDI C. Application of Brazilian-pine fruit coat as a biosorbent to removal of reactive red 194 textile dye from aqueous solution. Kinetics and equilibrium study. *J. Hazard. Mater.* **155**, 536, **2008**.
48. KARAGOZ S., TAY T., UCAR S., ERDEM M. Activated carbons from waste biomass by sulfuric acid activation and their use on methylene blue adsorption. *Bioresource Technol.* **99**, 6214, **2008**.
49. CHATTERJEE S., WOO S.H. The removal of nitrate from aqueous solutions by chitosan hydrogel beads. *J. Hazard. Mater.* **164**, 1012, **2009**.
50. CRINI G., BADOT P.-M. Sorption processes and pollution. Conventional and non-conventional sorbents for pollutant removal from wastewaters, Presses universitaires de Franche-Comté, France, **2010**.
51. GARCIA E.R., MEDINA R.L., LOZANO M.M., PÉREZ I.H., VALERO M.J., FRANCO A.M.M. Adsorption of Azo-Dye Orange II from Aqueous Solutions Using a Metal-Organic Framework Material: Iron-Benzenetricarboxylate. *Materials* **7**, 8037, **2014**.
52. AMRHAR O., NASSALI H., ELYOUBI M.S. Adsorption of a cationic dye, Methylene Blue, onto Moroccan Illitic Clay. *J. Mater. Environ. Sci.* **6** (11), 3054, **2015**.
53. HUANG C.H., CHANG K.P., OU H.D., CHIANG Y.C., WANG C.F. Adsorption of cationic dyes onto mesoporous silica. *Micropor. Mesopor. Mat.* **141**, 102, **2011**.